Frontiers in Bioscience Landmark

Front. Biosci. (Landmark Ed) **2023**; 28(8): 179
https://doi.org/10.31083/j.fbl2808179

Original Research

Integrated Bioinformatic Analyses Reveal Immune Molecular Markers and Regulatory Networks for Cerebral Ischemia-Reperfusion

Qixin Guo[1,2,†], Anning Du[2,†], Jiayue Wang[3,†], Luyang Wang[2], Xu Zhu[2], Xin Yue[2], Shengen Liao[2], Mengsha Shi[2], Qiang Qu[2], Iokfai Cheang[2], Xinli Li[2], Hui Pang[4,*], Guoxin Tong[1,*]

[1]Department of Cardiology, Affiliated Hangzhou First People's Hospital, Zhejiang University, School of Medicine, 310006 Hangzhou, Zhejiang, China
[2]Department of Cardiology, The First Affiliated Hospital of Nanjing Medical University, 210029 Nanjing, Jiangsu, China
[3]Department of Rehabilitation Medicine, The First Affiliated Hospital of Nanjing Medical University, 210029 Nanjing, Jiangsu, China
[4]Department of Cardiology, Xuzhou Central Hospital, Xuzhou School of Clinical Medicine of Nanjing Medical University, 221009 Nanjing, Jiangsu, China
*Correspondence: njmupanghui@126.com (Hui Pang); njmutongguoxin@126.com (Guoxin Tong)
[†]These authors contributed equally.
Academic Editor: Ricardo Jorge Pinto Araujo
Submitted: 16 November 2022 Revised: 14 February 2023 Accepted: 28 February 2023 Published: 25 August 2023

Abstract

Background: Cerebral ischemia-reperfusion injury (CIR) following a stroke results in secondary damage and is a leading cause of adult disability. The present study aimed to identify hub genes and networks in CIR to explore potential therapeutic agents for its treatment. **Methods**: Differentially expressed genes based on the GSE23163 dataset were identified, and weighted gene co-expression network analysis was performed to explore co-expression modules associated with CIR. Hub genes were identified by intersecting immune gene profiles, differentially expressed genes, and modular genes. Gene Ontology, Kyoto Encyclopedia of Genes and Genomes pathway, and transcription factor-microRNA-gene regulatory network analyses were then conducted in selected crucial modules. Subsequently, their expression levels in animal models were verified using real-time quantitative polymerase chain reaction and Western blotting. Finally, potential drug molecules were screened for, and molecular docking simulations were performed to identify potential therapeutic targets. **Results**: Seven hub genes—namely, *Ccl3*, *Ccl4*, *Ccl7*, *Cxcl1*, *Hspa1a*, *Cd14*, and *Socs3*—were identified. Furthermore, we established a protein interaction network using the STRING database and found that the core genes selected through the cytohubba plugin remained consistent. Animal experiments showed that at the transcriptional level, all seven genes showed significant differences ($p < 0.001$, fold change vs sham, 5–200). At the translational level, however, only *Ccl3*, *Ccl4*, *Ccl7*, *Hspa1a*, and *Socs3* showed significant differences, while *Cxcl1* and *Cd14* did not. Nifedipine, with the highest predicted score, was identified as a therapeutic agent and successfully docked with the protein encoded by the hub genes. **Conclusions**: The expression of *Ccl3*, *Ccl4*, *Ccl7*, *Hspa1a*, and *Socs3* was significantly different in CIR tissues compared to normal tissues both at the transcriptional and translational levels. Systems biology approaches indicated that these could be possible CIR marker genes, providing a stepping stone for further experimental studies.

Keywords: cerebral ischemia-reperfusion; differentially expressed gene; hub genes; ischemic stroke; molecular docking; nifedipine; weighted gene co-expression network analysis

1. Introduction

Ischemic stroke is the dominant cause of acquired adult disability and premature death, accounting for up to 75% of all strokes and 50% of stroke-related deaths [1,2]. Ischemic stroke commonly arises from a sudden reduction or obstruction of cerebral blood flow; it interrupts the transfer of oxygen and essential nutrients to the brain required to maintain metabolism [3]. Currently, well-established therapeutic approaches for ischemic stroke are confined to intravenous thrombolysis and endovascular thrombectomy, the efficacies of which are highly time-dependent [4–6]. Cerebral blood flow re-establishment via intravenous thrombolysis and endovascular thrombectomy or both can salvage the ischemic hypoxic state of brain tissue, but it also leads to further tissue damage and dysfunction, known as cerebral ischemia-reperfusion injury (CIR) [7].

Multiple signaling pathways and biological processes that form a complex signaling network are involved in the pathophysiology of CIR [8,9]. Of these, oxidative stress and inflammation have been explored extensively. In particular, inflammation is a prime target for the development of new stroke and CIR therapies [10]. However, the exact role of inflammation in the pathophysiology of stroke and CIR remains controversial. A severe inflammatory response and infiltration of immune cells, such as neutrophils, macrophages, and lymphocytes [10–13], caused by CIR may result in systemic inflammatory responses or multiple organ dysfunction syndromes [9,14]. In contrast, several studies have argued that infiltration of certain immune

cells (particularly regulatory T cells) might have a protective effect during CIR [15,16]. Therefore, understanding the molecular mechanisms of immune cell infiltration during CIR is required to unravel its precise molecular mechanisms.

Recent advances in genomics and bioinformatics have provided new perspectives on the molecular mechanisms of CIR. For instance, Cheng *et al*. [17] reported the TLR4/MYD88 inflammatory signaling pathway as a novel therapeutic target for CIR via high-throughput RNA-sequencing transcriptome analysis. Zhang *et al*. [18] compared differentially expressed circular RNAs in the brain tissue of rats afflicted with CIR and reported circ-camk4 as a pivotal biomolecule in apoptosis signaling pathways. However, these methods focus only on the effects of a single transcription factor (TF)/molecule. Therefore, the relationships between the entire gene network and clinical disease cannot be established [19,20]. Nonetheless, these situations can be avoided using weighted gene co-expression network analysis (WGCNA), an updated systems biology method for identifying relationships between genes and phenotypes based on RNA-sequencing or microarray data [21]. The WGCNA can transform clusters of genes into co-expression modules and identify genes, networks, and phenotypes that have high connectivity or correlation with one another [20,22]. This method has widely been used to study various biological processes and explore potential therapeutic targets for many diseases [21,23,24].

This study aims to identify and validate hub genes and networks in CIR based on the gene expression profiling dataset GSE23163 from the Gene Expression Omnibus (GEO) database. The findings of this study can contribute to revealing the related molecular mechanisms and potential therapeutic targets of CIR.

2. Materials and Methods

2.1 Study Workflow

The overall workflow of this study is shown in Fig. 1. Briefly, the GSE23163 dataset was collected from the GEO database (http://www.ncbi.nlm.nih.gov/geo) and converted into a suitable format for analysis, and differentially expressed genes (DEGs) were identified. Subsequently, the dataset was subjected to WGCNA to delineate the modular gene nest most associated with CIR, followed by the immune infiltration analysis. Then the pivotal genes were identified by intersecting the prepared immune gene profiles, DEGs, and modular genes. The differential expression of pivotal genes was verified after successfully constructing a CIR animal model. Afterward, a protein interaction network (modeling of microRNA-DEGs and transcription factor (TF)-DEGs) was constructed. Finally, a molecular docking simulation of potential small drug molecules to treat CIR was performed.

2.2 Gene Expression Datasets

The gene expression profiling dataset GSE23163 (annotation platform GPL6885) contained 48 CIR and 16 sham surgery samples. The downloaded raw data were converted into gene names with the assistance of probes. Then, the sequencing data were log transformed and normalized using the "sva" package into expression datasets that could be directly analyzed.

2.3 Identification of DEGs and Gene Set Enrichment Analysis (GSEA)

The DEGs between the CIR and sham samples were determined using the "limma" package. The p-values lower than 0.05 and logFC absolute values >1 were defined as significant, and the magnitude of logFC values and p-values were visualized hierarchically as volcano plots and heat maps. Gene Ontology (GO) and Kyoto Encyclopedia of Genes and Genomes (KEGG) analyses were performed on CIR and normal samples using the GSEA 4.2.3 software (Cambridge, MA, USA) http://www.gsea-msigdb.org/gsea/index.jsp. The random combination was set at 1000 times. To investigate the CIR-related risk signature's molecular characteristics and pathways, we conducted GSEA to display differences in 159 gene sets and 186 KEGG gene sets. Gene sets that had enrichment scores with a normalized p-value < 0.05 and a false discovery rate of <0.25 were considered significantly enriched.

2.4 Protein–Protein Interactions (PPI) and Gene Regulatory Network Analyses

PPIs are a target of cell biology research and a prerequisite for systems biology studies. PPI networks are defined as graphs where nodes and edges represent proteins and their interactions, respectively [25,26]. To investigate the potential molecular mechanisms of CIR from the perspective of protein interactions, a PPI network of DEGs was constructed using the STRING database (https://string-db.org/) and visualized using Cytoscape (https://cytoscape.org/) [27]. The "cytohubba" (sorting by "degree" size) and "MCODE" (basic cut-off, criterion degree cutoff = 2, node score cutoff = 0.2, k-core = 2, maximum depth = 100) plugins were used to further validate the plausibility of the hub genes [28]. TF-miRNA co-regulatory interactions were collected from the RegNetwork repository (http://www.regnetworkweb.org) to detect miRNAs and TFs regulating the DEG of interest at the post-transcriptional and transcriptional levels. The DEG-miRNA network was validated using the experimentally validated miRNA-target interactions databases TarBase and miRTarBase, based on the selected genes, and checked on the platform. The DEG-miRNA target genes were validated using the JASPAR (https://jaspar.genereg.net/) and GEPIA (http://gepia.cancer-pku.cn/) databases.

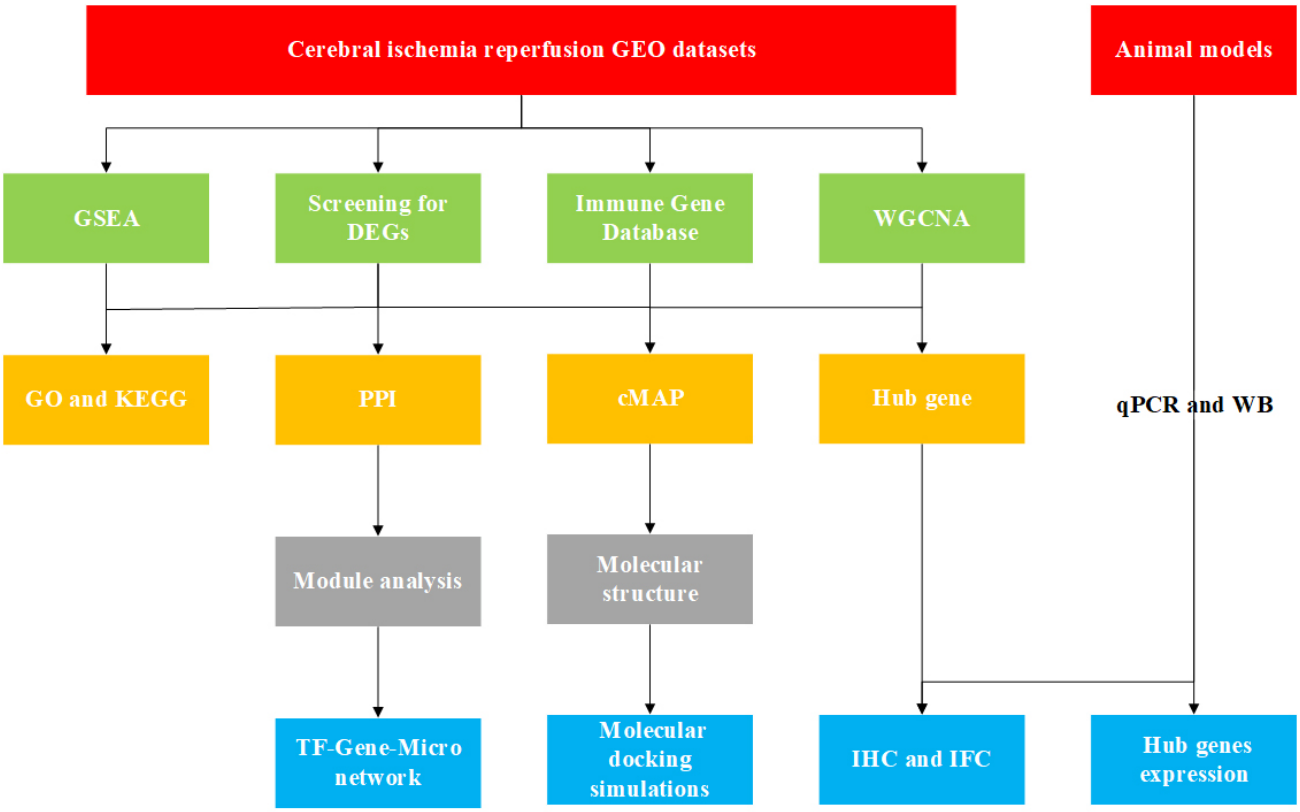

Fig. 1. Study workflow. This study includes seven key stages. In phase I, an appropriate dataset was collected and converted into a format suitable for analysis. In phase II, DEGs were delineated in the target dataset. In phase III, the modular gene nest most associated with CIR was targeted by WGCNA. In Phase IV, the dataset was subjected to immune infiltration analysis. Subsequently, the prepared immune gene profiles, DEGs, and modular genes were intersected to obtain pivotal genes. In Phase V, the differential expression of pivotal genes was verified after successfully constructing a CIR animal model. In Phase VI, a protein interaction network (modelling of miRNA-DEGs and TF-DEGs) was constructed. Finally, in Phase VII, the molecular docking simulation of potential small drug molecules to treat CIR was performed. DEGs, differentially expressed genes; miRNA, microRNA; GEO, Gene Expression Omnibus; GO, Gene Ontology; PPI, protein–protein interaction; cMap, Connectivity Map; KEGG, Kyoto Encyclopedia of Genes and Genomes; GSEA, Gene Set Enrichment Analysis; WGCNA, Weight gene co-expression network analysis; qPCR, quantitative real-time PCR; IHC, immunohistochemistry; IFC, immunofluorescence staining; WB, Western blotting.

2.5 WGCNA

The relevant network was built using the "WGCNA" package to identify the key molecules of CIR. The main steps were: (i) A power of $\beta = 7$ was selected according to the scale-free topology criterion; (ii) Hierarchical clustering trees were constructed based on the weighted correlation coefficients of the genes, and the related modules were merged; (iii) Identification of hub gene clusters based on module-phenotype correlations; (iv) GO and KEGG enrichment analyses according to the modular gene ensemble.

2.6 Immuno-Infiltration Analysis

CIBERSORT is a gene expression profiling-based method used for quantifying immune cell infiltration in tissues. The CIBERSORT analysis is based on LM22, the annotated gene signature matrix comprising 22 functionally defined immune cell subtypes. The 22 immune cell types included macrophage subsets (M0, M1, and M2), T cells (CD8+ T cells, naïve CD4+ T cells, memory resting CD4+ T cells, memory activated CD4+ T cells, Tfh cells, regulatory T cells, and γ δ T cells), natural killer cells (resting and activated), mast cells (resting and activated), B cells (naive and memory), dendritic cells (resting and activated), monocytes, plasma cells, neutrophils, and eosinophils. In the present study, we downloaded the *LM22 gene* matrix from the CIBERSORT portal (http://cibersort.stanford.edu/). To improve the accuracy of the inverse fold product algorithm, the *p*-value and root mean square error of CIBERSORT were counted for each sample file.

2.7 Identification and Validation of Target TF

The sequences of potential hub genes corresponding to TF-binding sites were obtained from the UCSC database (https://genome.ucsc.edu/). The sequence information was then imported into JASPAR to retrieve possible

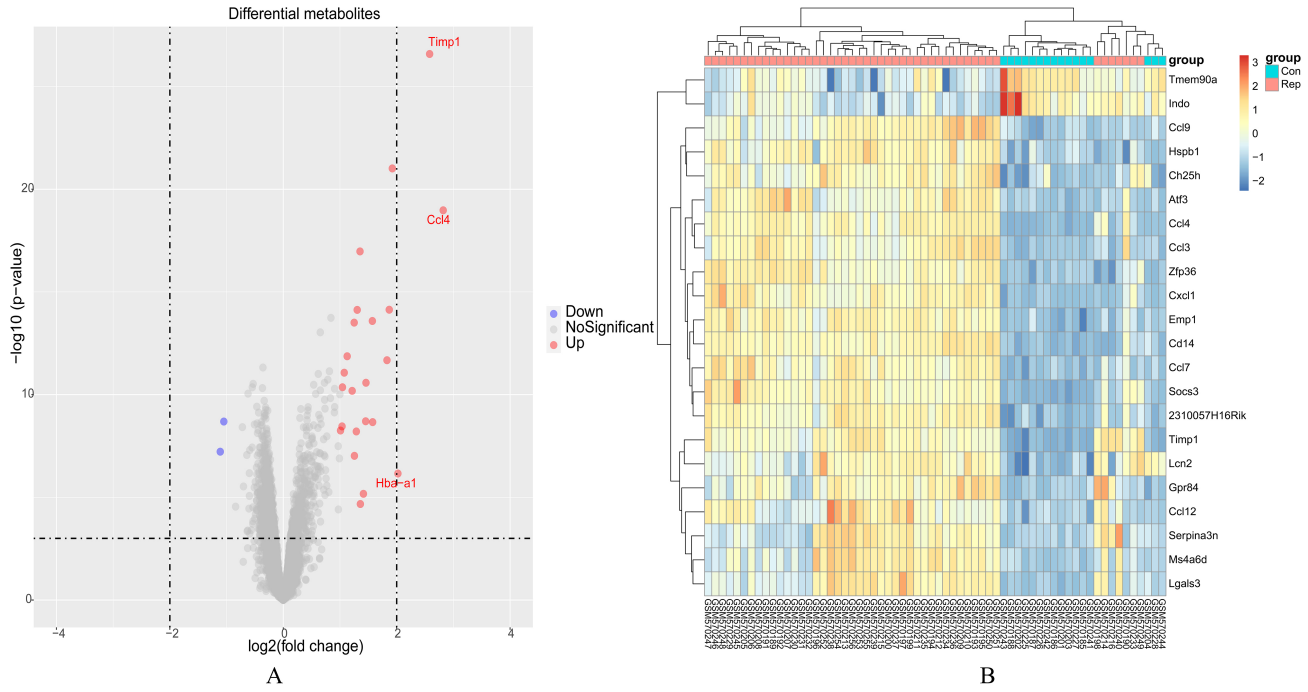

Fig. 2. Identification of DEGs in CIR. Graphical visualization of the results of the variance analysis. (A,B) Gene expression profiles of GSE23163 are visualized in (A) volcano plots and (B) heat maps. DEGs, differentially expressed genes; CIR, cerebral ischemia-reperfusion injury; Con, Control group; Rep, Ischemia-reperfusion group.

TFs. Candidates that did not meet the inclusion criteria ($p < 0.000001$) were eliminated based on their transcriptional direction and binding power. Finally, expression correlation was verified using the GEPIA database.

2.8 Identification and Molecular Docking Simulation of Potential Therapeutic Molecules

The molecular docking simulations were performed using the following steps. First, the up- and downregulated DEGs were introduced into the clue.io platform to screen the therapeutic molecules. Then, the two- and three-dimensional structures of the compounds were extracted from the PubChem database (https://pubchem.ncbi.nlm.nih.gov/). Afterward, the structure of the protein receptor encoded by the target gene was elucidated by screening the molecules in the UniProt (https://www.uniprot.org/) and PDB databases (https://www.rcsb.org/). Finally, CHEM 3D (PerkinElmer, Waltham, MA, USA) and AutoDock Vina-1.5.7 (The Scripps Research Institute, SanDiego, CA, USA) were used for the spatial processing of ligands and receptors, and PYMOL (http://www.pymol.org/pymol) was used for docking and annotating the drug and protein molecules.

2.9 Middle Cerebral Artery Occlusion and Reperfusion (MCAO/R) Surgical Procedure

All animal experiments were performed in accordance with protocols approved by the Ethics Committee of Nanjing Medical University and complied with the Guidelines of Laboratory Animals for Biomedical Research published by the National Institutes of Health (NIH publication, revised in 2011).

Eight-week-old male C57BL/6J mice (n = 12) weighing 20–25 g were obtained from Beijing Weitong Lihua Company (Beijing, China). The mice were housed under a 12-hour light/dark cycle with free access to food and water. The MCAO/R model was established as described previously, with minor modifications [29]. Briefly, mice were anesthetized with 2% isoflurane and placed on a heating pad to maintain body temperature at 37 °C. The left common carotid and external carotid arteries were exposed and ligated permanently to block blood flow. A small incision was made in the common carotid artery, from which a monofilament nylon suture (final tip diameter 0.20 ± 0.01 mm, Cat.1620A4, Beijing Cinontech Co. Ltd, Beijing, China) was inserted and advanced towards the internal carotid artery. The internal carotid artery was occluded at the level of the middle cerebral artery branches for 60 min. The suture was then carefully removed to allow reperfusion for 24 h. Mice with excessive bleeding or that died within 24 h after reperfusion were excluded from the study data.

2.10 Neurological Deficit Score Evaluation

The neurological deficit score of ischemic mice was evaluated 24 h after reperfusion based on the five-point scale model established previously [30]. Score 0: no neurological deficit. Score 1: failure to extend the contralateral

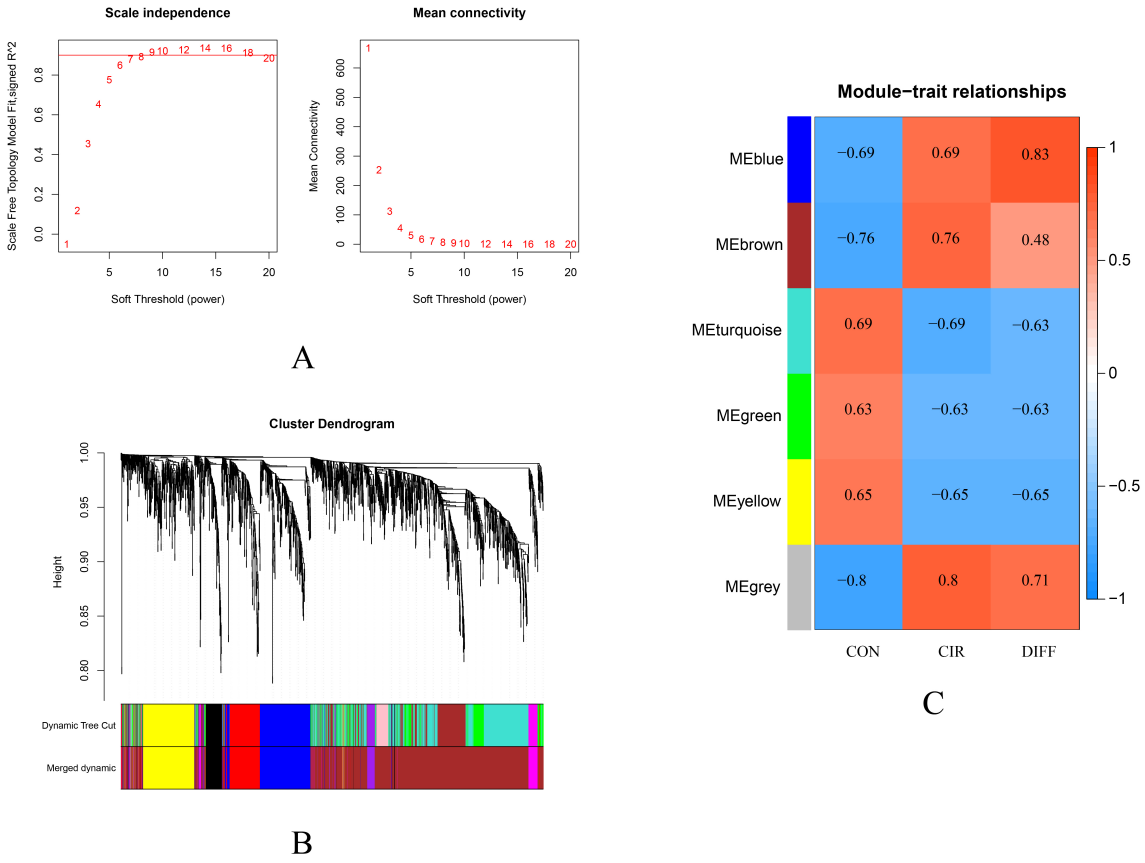

Fig. 3. Gene co-expression modules. Screening for the gene module that best matches the trait. (A) Scale-free index and mean connectivity analyses for various soft-threshold powers. (B) Hierarchical cluster dendrogram of CIR-related genes based on one dissimilarity measure. The color band shows the results obtained from the automatic single-block analysis. (C) Module–trait relationships in CIR; each cell contains the corresponding correlation and *p*-value. The value between –1 and 1 represents the correlation between the module and clinical features.

forelimb. Score 2: circling the contralateral side. Score 3: falling to the contralateral side. Score 4: no spontaneous motor activity or death.

2.11 Measurement of Cerebral Infarct Volume Percentage Using 2,3,5-Triphenyl Tetrazolium Chloride Staining

The mice were euthanized 24 h after reperfusion, and their brains were quickly removed. Five 2 mm-thick consecutive coronal slices were made and incubated in 2% 2,3,5-Triphenyl tetrazolium chloride (Cat.T8877, Sigma-Aldrich, St. Louis, MO, USA) solution at 37 °C for 30 min in the dark. Afterward, the slices were imaged using a digital camera, and the infarct area of each slice was measured using ImageJ software.1.8.0 (National Institutes of Health, Bethesda, MD, USA). The percentage of each cerebral infarct volume was calculated according to the following formula: total cerebral infarct volume/total brain volume × 100.

2.12 RNA Extraction, Reverse Transcription, and Real-Time Polymerase Chain Reaction (PCR)

Total RNA from the cortex tissues of the removed brains was isolated using TRIzol reagent (Cat.9208, Takara, Takara Bio, Inc., Otsu, Shiga, Japan), following the manufacturer's protocol. Total RNA (500 ng) was reversely transcribed into cDNA using PrimeScriptTM RT Master Mix (Cat. RR036A; Takara, Japan). Real-time PCR was performed on the system using SYBR Green dye (Cat.11199ES03, Yeasen, Shanghai, China). The following primer pairs for murine were used: C-C motif chemokine ligand 3 (*Ccl3; Mus*): 5′-CCAGCCAGGTGTCATTTT-3′, 5′-GCATTCAGTTCCAGGTCAG-3′; *Ccl4* (*Mus*):5′-AACCTAACCCCGAGCAA-3′, 5′-AAACAGCAGGAAGTGGGA-3′; *Ccl7* (*Mus*):5′-CAGAAGTGGGTCGAGGAG-3′, 5′-AAGAACAGCGGTGAGGAA-3′; CXC motif chemokine ligand 1 (*Cxcl1;* (*Mus*):5′-AACCGAAGTCATAGCCACA-3′, 5′-GGGGACACCTTTTAGCATC-3′; *Cd14* (*Mus*):5′-CTGTCTTTCACTGGGCTGA-3′, 5′-GCTCATCTGGGCTAGGG-3′; Suppres-

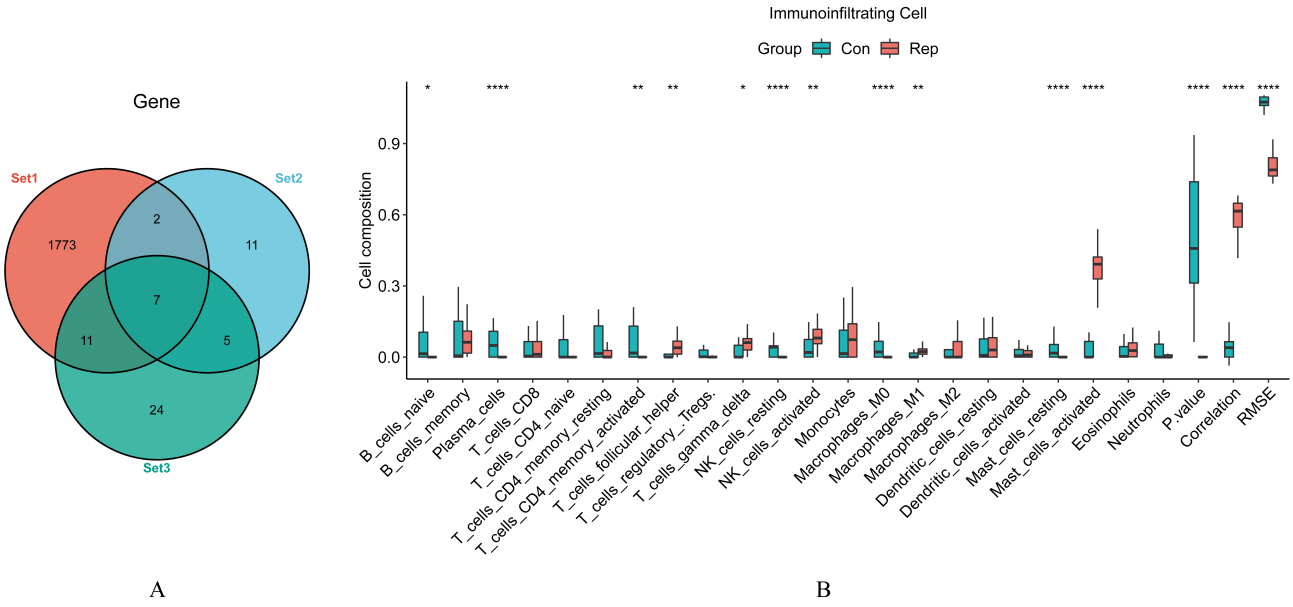

Fig. 4. Immune infiltration analysis and intersection dataset. To accurately evaluate the composition of immune cells and the establishment of key molecules in the microenvironment after ischemia reperfusion. (A) Venn diagram of the intersection of the brown module (MEbrown), immune genes, and DEGs. (B) The proportion of 22 types of immune cells corresponding to immune infiltration analysis. *$p < 0.05$, **$p < 0.01$, ****$p < 0.0001$.

sor of cytokine signaling (*Socs3*; *Mus*):5′-GTCGG TCGCCTCTCCTC-3′, 5′-ATCTGCCCCTGGCTCAC-3′; *Hspa1a* (*Mus*):5′-GCTTGTGTCGGGTCCTTC-3′, 5′-TGCTGTCACTTCACCTCCA-3′; *Gapdh* (*Mus*):5′-AGGTCGGTGTGAACGGATTTG-3′, 5′-TGTAGACCA TGTAGTTGAGGTCA-3′.

2.13 Protein Expression Analysis in Brain Tissue

Total protein was extracted from tissues according to the instructions for Radioimmunoprecipitation Assay Lysis Buffer (Beyotime, Shanghai, China). Next, total protein concentration was measured using the BCA assay (Beyotime, China). Total proteins were separated by Sodium Dodecyl Sulfate Polyacrylamide Gel Electrophoresis on 12.5% polyacrylamide gels and electrophoretically transferred to PVDF membranes, which were subsequently sealed with 5% BSA. The membranes were incubated overnight at 4 °C with diluted primary antibodies for Ccl3 (1:1000 dilution, Affinity Biosciences, Cincinnati, OH, USA), Ccl4 (1:1,000 dilution, Affinity Biosciences, USA), Ccl7 (1:1,000 dilution, Affinity Biosciences, USA) Cxcl1 (1:1000 dilution, Affinity Biosciences, USA), Hapa1a (1:1000 dilution, Wanleibio, Shenyang, China), Cd14 (1:1000 dilution, Wanleibio, China), and Socs3 (1:1000 dilution, Wanleibio, China). The membranes were then further incubated with secondary antibody (ZSGB-BIO, Beijing, China) for 1 hour at room temperature. Finally, the protein bands were analyzed and quantified using ImageJ software (National Institutes of Health, Bethesda, MD, USA).

The Human Protein Atlas Database (HPAD; https://www.proteinatlas.org/) was used to verify the immunohistochemistry of brain tissues and fluorescence staining of cells. This database is helpful for systematically studying the transcription and translation levels of coding genes in different tissue types. The localization of target genes in tissues and cell protein expression was further analyzed.

3. Results

3.1 CIR-Related Immune Genes

A total of 25 DEGs associated with CIR were identified in the GSE23163 dataset, of which 23 were upregulated, and 2 were downregulated. Genes with a |logFC| of >2 were additionally labeled in the volcano plot, namely *CCl4* and *Timp1*. The difference in expression between the CIR and sham groups was also observed in the heatmap (Fig. 2).

Based on WGCNA, the gene nests were divided into six modules, each with a specific color. The correlation coefficients of the modules were 0.69 (MEblue, $p < 0.001$), 0.76 (MEbrown, $p < 0.001$), –0.69 (MEturquoise, $p < 0.001$), –0.63 (MEgreen, $p < 0.001$), –0.65 (MEyellow, $p < 0.001$), and 0.8 (MEgrey, $p < 0.001$). The MEbrown module comprising 47 genes contained the most relevant gene set for CIR (Fig. 3).

Box line plot demonstrated significant infiltration in 11 of the 22 immune cells in CIR mice compared to that in normal control mice. However, medium B cell memory, T cell CD8, T cell CD4 naïve, T cell CD4 memory resting, T cell regulatory Tregs, monocytes, macrophages M2,

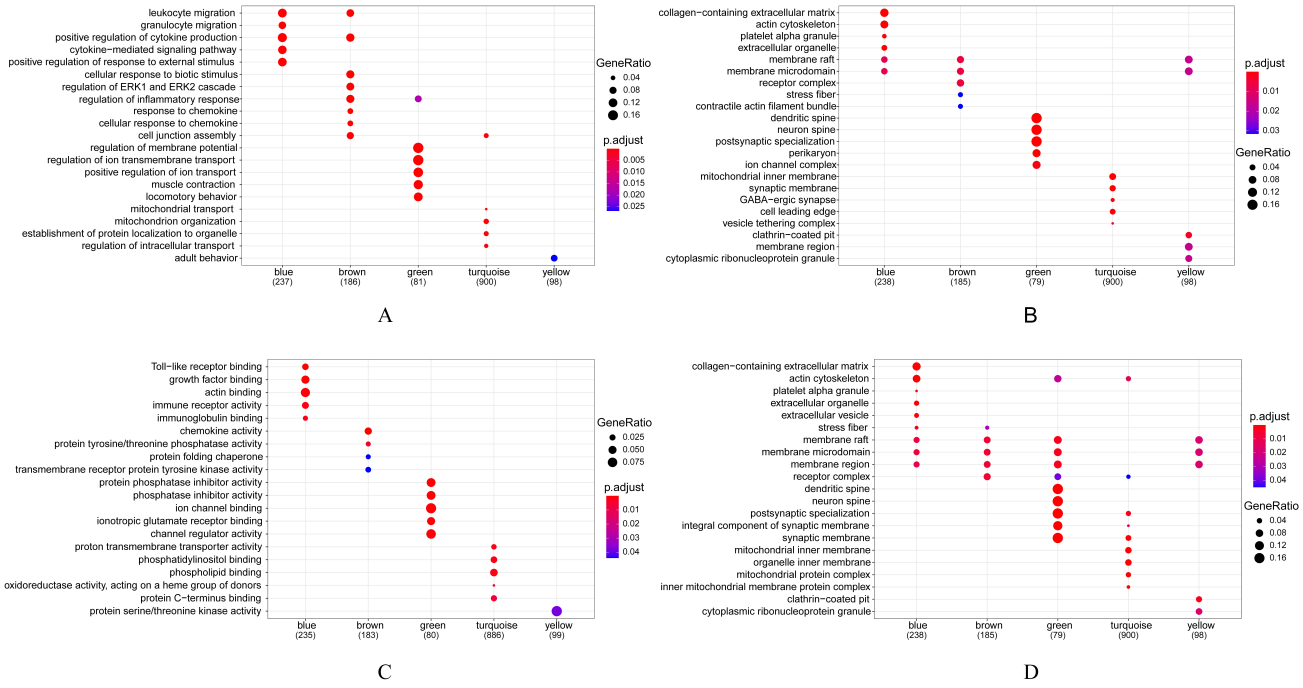

Fig. 5. Enrichment analyses of gene modules. Enrichment analysis of individual modules distinguished by WGCNA, including blue, brown, green, turquoise and yellow. Enrichment analyses of gene modules for (A) biological process; (B) cell component; (C) molecular function; and (D) KEGG pathway. KEGG, Kyoto Encyclopedia of Genes and Genomes.

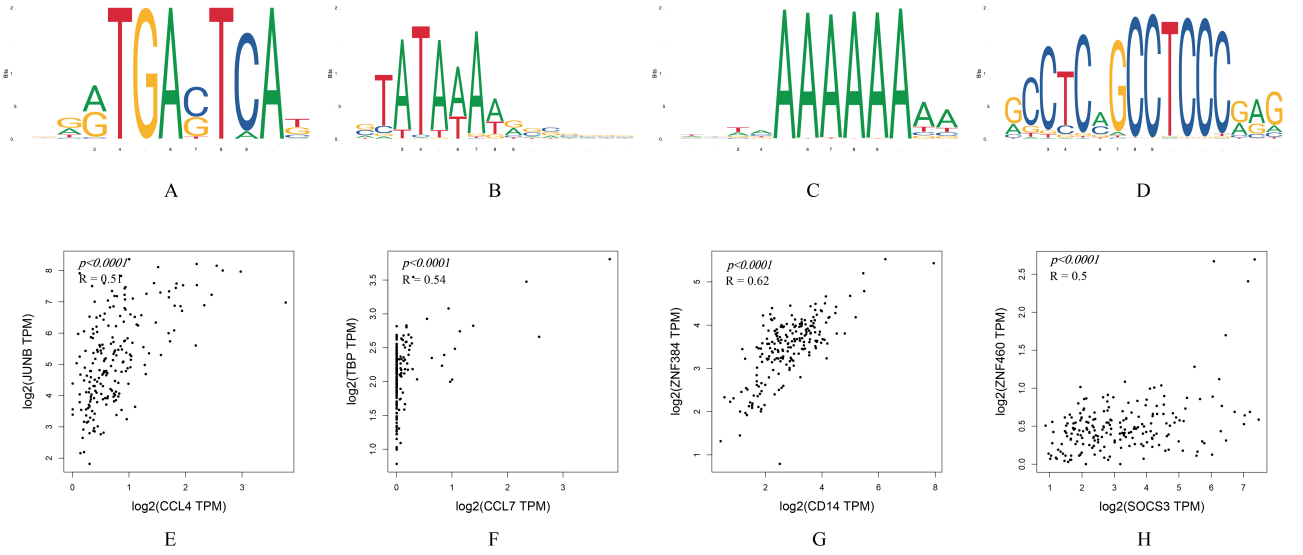

Fig. 6. Binding sites of transcription factors and expression correlation verification. After initial prediction of potential regulatory molecules, expression correlation of transcription factors and regulated genes is verified in public databases. (A) Binding site of JUNB. (B) Binding site of TBP. (C) Binding site of ZNF384. (D) Binding site of ZNF460. (E–H) Correlations of the expression levels of (E) *JunB* and *Ccl4*; (F) *Tbp* and *Ccl7*; (G) *Znf384* and *Cd14*; (H) and *Znf460* and *Socs3* genes in myocardial tissue.

dendritic cells resting, activated dendritic cells, eosinophils, and neutrophils were not infiltrated (Fig. 4). The intersection of the immune gene dataset (containing 1793 known immune-related genes), DEGs (n = 25), and MEbrown module genes (n = 47 phenotypically related genes) identified seven pivotal genes, including *Ccl3*, *Ccl4*, *Ccl7*, *Cxcl1*, *Hspa1a*, *Cd14*, and *Socs3*.

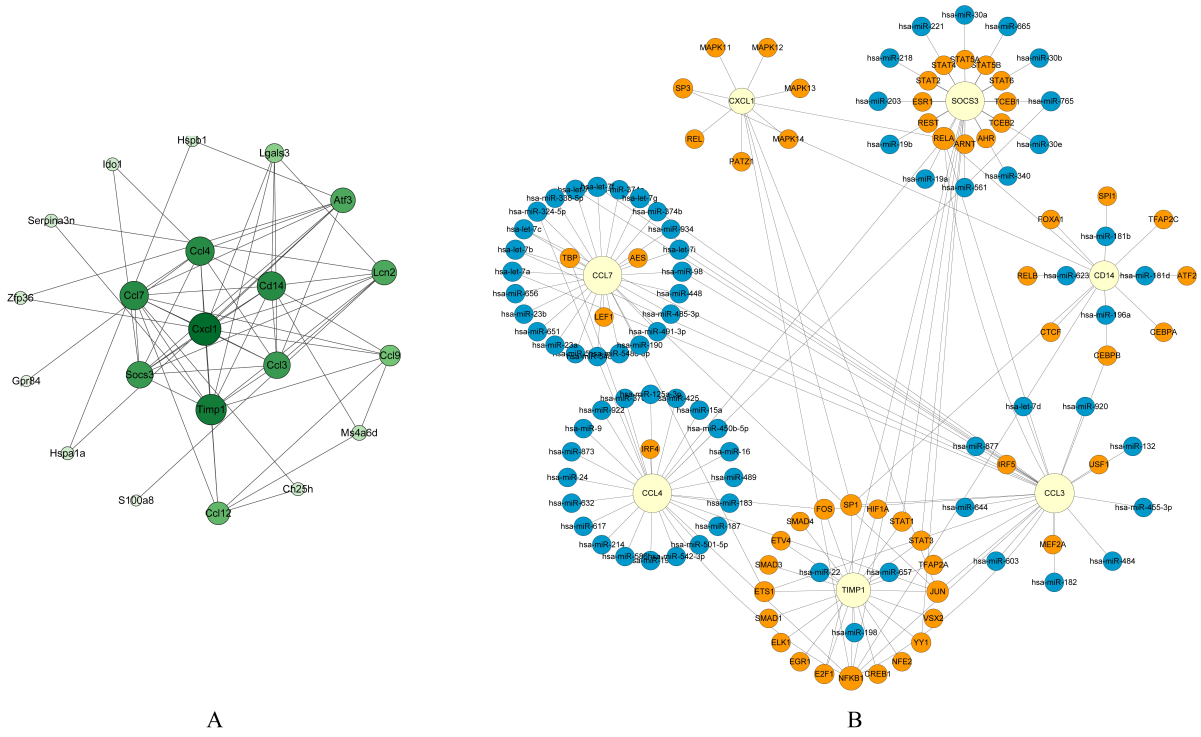

Fig. 7. PPI and TF-gene- miRNA networks. Constructing and visualizing regulatory networks through Cytoscape. (A) PPI network constructed using identified DEGs. Nodes represent DEGs, and edges represent the connection between DEGs. The depth of the color and the size of the circle reflects the degree of connectivity. (B) The pale-yellow nodes represent genes, the orange nodes represent TFs, the blue nodes represent miRNA, and the connecting lines represent the regulatory relationship between them. PPI, protein-protein interaction; TF, transcription factor; miRNA, microRNA; DEGs, differentially expressed genes.

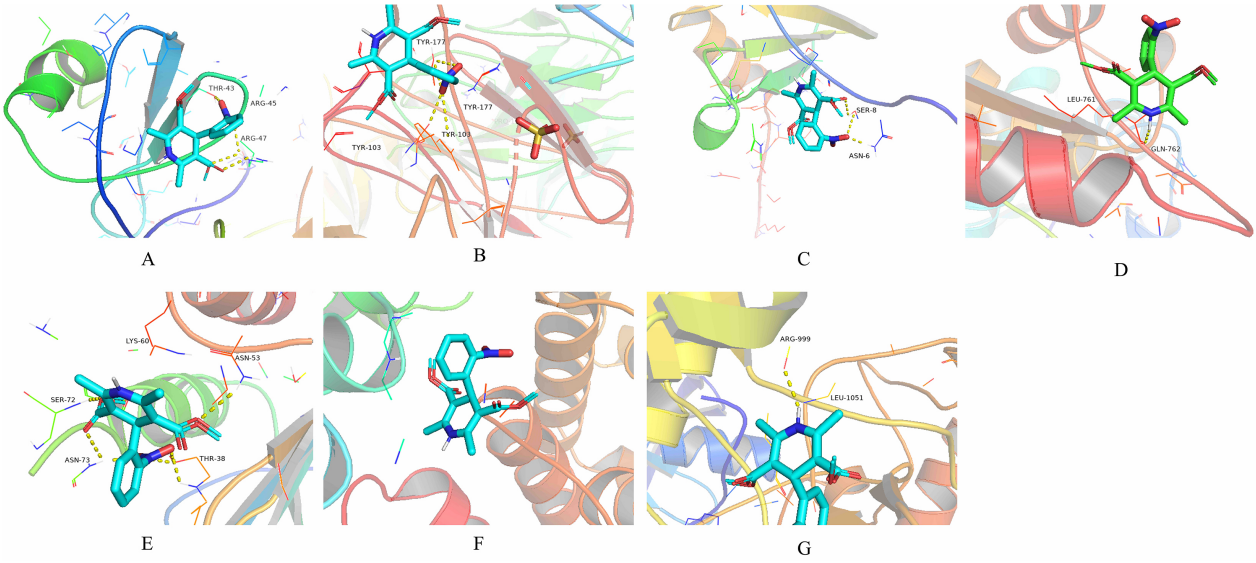

Fig. 8. Molecular docking simulations with nifedipine. Molecular docking of the screened small molecules for possible therapeutic use with the proteins encoded by each target gene, and if a stable binding site can be formed, it indicates a possible therapeutic effect. (A) CCL3. (B) CCL4. (C) CCL7. (D) CD14. (E) CXCL1. (F) HSPA1A. (G) SOCS3.

Table 1. GO and KEGG pathway enrichment analysis of DEGs in the CIR and CON samples.

NAME	SIZE	ES	NES	NOM *p*-value	FDR *q*-value	LEADING EDGE
GOBP_EOSINOPHIL_CHEMOTAXIS	15	0.9095553	2.5891242	<0.0001	<0.0001	tags = 47%, list = 0%, signal = 47%
GOBP_EOSINOPHIL_MIGRATION	19	0.8402558	2.585179	<0.0001	<0.0001	tags = 37%, list = 0%, signal = 37%
GOBP_ESTABLISHMENT_OF_PIGMENT_GRANULE_LOCALIZATION	20	–0.7178649	–2.1726959	<0.0001	<0.0001	tags = 45%, list = 8%, signal = 49%
GOBP_MODULATION_OF_EXCITATORY_POSTSYNAPTIC_POTENTIAL	29	–0.7099049	–2.31776	<0.0001	<0.0001	tags = 72%, list = 21%, signal = 91%
GOBP_MYD88_DEPENDENT_TOLL_LIKE_RECEPTOR_SIGNALING_PATHWAY	20	0.74633956	2.3537517	<0.0001	<0.0001	tags = 45%, list = 4%, signal = 47%
GOBP_NEUTROPHIL_CHEMOTAXIS	72	0.7066228	2.996933	<0.0001	<0.0001	tags = 39%, list = 8%, signal = 42%
GOBP_PIGMENT_GRANULE_LOCALIZATION	22	–0.7173519	–2.1862688	<0.0001	<0.001	tags = 45%, list = 8%, signal = 50%
GOBP_POSITIVE_REGULATION_OF_ACUTE_INFLAMMATORY_RESPONSE	22	0.7284434	2.3110445	<0.0001	<0.001	tags = 50%, list = 6%, signal = 53%
GOBP_POSITIVE_REGULATION_OF_CYTOKINE_PRODUCTION_INVOLVED_IN_INFLAMMATORY_RESPONSE	16	0.714022	2.0749276	<0.0001	0.002	tags = 75%, list = 15%, signal = 88%
GOBP_POSITIVE_REGULATION_OF_EXCITATORY_POSTSYNAPTIC_POTENTIAL	21	–0.7254008	–2.1654482	<0.0001	<0.0001	tags = 71%, list = 21%, signal = 90%
GOBP_POSITIVE_REGULATION_OF_INTERLEUKIN_1_BETA_PRODUCTION	37	0.7422596	2.7434237	<0.0001	<0.0001	tags = 46%, list = 7%, signal = 49%
GOBP_POSITIVE_REGULATION_OF_INTERLEUKIN_8_PRODUCTION	43	0.71923137	2.7636735	<0.0001	<0.0001	tags = 40%, list = 7%, signal = 42%
GOBP_POSITIVE_REGULATION_OF_LEUKOCYTE_ADHESION_TO_VASCULAR_ENDOTHELIAL_CELL	20	0.7151746	2.2081444	<0.0001	<0.001	tags = 40%, list = 7%, signal = 43%
GOBP_POSITIVE_REGULATION_OF_LYMPHOCYTE_CHEMOTAXIS	16	0.7077763	2.1062818	<0.0001	0.0014	tags = 25%, list = 0%, signal = 25%
GOBP_REGULATION_OF_LYMPHOCYTE_CHEMOTAXIS	20	0.75301516	2.3239057	<0.0001	<0.001	tags = 30%, list = 0%, signal = 30%
GOBP_RESPONSE_TO_PROTOZOAN	15	0.80573744	2.3104577	<0.0001	<0.001	tags = 40%, list = 2%, signal = 41%
GOBP_T_HELPER_17_CELL_DIFFERENTIATION	22	0.71492696	2.2967973	<0.0001	<0.001	tags = 27%, list = 2%, signal = 28%
GOBP_TOLERANCE_INDUCTION	17	0.71679676	2.1241786	<0.0001	0.0011	tags = 53%, list = 12%, signal = 60%
GOCC_CLATHRIN_VESICLE_COAT	19	–0.71680665	–2.1362166	<0.0001	<0.001	tags = 68%, list = 22%, signal = 87%
GOCC_CYTOCHROME_COMPLEX	24	–0.70855844	–2.1915617	<0.0001	<0.001	tags = 67%, list = 17%, signal = 81%
GOCC_NADH_DEHYDROGENASE_COMPLEX	33	–0.7028937	–2.3509545	<0.0001	<0.0001	tags = 79%, list = 22%, signal = 101%
GOCC_PHAGOPHORE_ASSEMBLY_SITE	15	–0.7261254	–2.0345428	<0.0001	0.0023	tags = 60%, list = 17%, signal = 72%
GOMF_CCR_CHEMOKINE_RECEPTOR_BINDING	25	0.7649167	2.5623467	<0.0001	<0.0001	tags = 44%, list = 7%, signal = 47%
GOMF_CHEMOKINE_ACTIVITY	30	0.75560206	2.6236312	<0.0001	<0.0001	tags = 50%, list = 7%, signal = 54%
GOMF_CHEMOKINE_RECEPTOR_BINDING	40	0.72412103	2.7034452	<0.0001	<0.0001	tags = 43%, list = 7%, signal = 46%
GOMF_NADPLUS_NUCLEOSIDASE_ACTIVITY	20	0.8115572	2.5249987	<0.0001	<0.0001	tags = 60%, list = 8%, signal = 65%
KEGG_LEISHMANIA_INFECTION	47	0.69171065	2.636909	<0.0001	<0.0001	tags = 38%, list = 7%, signal = 41%
KEGG_NOD_LIKE_RECEPTOR_SIGNALING_PATHWAY	40	0.68140006	2.507385	<0.0001	<0.0001	tags = 38%, list = 7%, signal = 40%
KEGG_SYSTEMIC_LUPUS_ERYTHEMATOSUS	32	0.66511315	2.3349216	<0.0001	<0.0001	tags = 47%, list = 10%, signal = 52%
KEGG_TYPE_I_DIABETES_MELLITUS	19	0.70135003	2.153117	<0.0001	<0.001	tags = 37%, list = 4%, signal = 38%

DEGs, differentially expressed genes; CIR, Cerebral ischemia-reperfusion; CON, control; ES, enrichment score; NES, normalized enrichment score; NOM *p*-value, nominal *p* value; FDR, false discovery rate; GO, Gene Ontology; KEGG, Kyoto Encyclopedia of Genes and Genomes; BP, biological process; CC, cellular component; MF, molecular function.

3.2 GO and KEGG Enrichment Analysis of Mebrown Module and Gene Sets

GO analysis (Fig. 5) demonstrated that the genes in the MEbrown module were involved in biological processes such as "cellular response to biotic stimulus", "regulation of ERK1 and ERK2 cascade", "regulation of inflammatory response", "response to chemokines", "cellular response to chemokines", and "cell junction assembly". The cellular component GO terms of these genes were enriched in "membrane rafts", "membrane microdomains", "receptor complexes", "stress fibers", and "contractile actin filament bundles". The molecular function terms were mainly enriched in "chemokine activity", "protein tyrosine/threonine phosphatase activity", "protein folding chaperone", and "transmembrane receptor protein tyrosine kinase activity".

KEGG analysis identified the enrichment of the pathways involved in "stress fibers", "membrane rafts", "membrane microdomains", "membrane regions", and "receptor complexes". The enrichment scores for CIR mice vs control mice were obtained by screening the genes based on their |normalized enrichment scores (NES)| >0.7, $p < 0.05$, and $q < 0.25$). The GSEA (**Supplementary Fig. 1**) identified enrichment of biological processes terms related to "regulation of acute inflammatory response", "regulation of eosinophils chemotaxis", "regulation of eosinophils migration", "regulation of lymphocyte chemotaxis", and "positive regulation of interleukin 1 β production". The identified cellular components terms were "clathrin-coated vesicle", "cytochrome complex", "NADH dehydrogenase complex", and "phagophore assembly site". The molecular function terms were "ccr chemokine receptor binding", "chemokine activity", "chemokine receptor binding", and "NADH+ nucleosidase activity". The KEGG-enriched pathways were related to "type 1 diabetes mellitus", "systemic lupus erythematosus", "the nod-like receptor signaling pathway", and "*Leishmania* infection". These results indicated a considerable similarity between the results of the enrichment analysis of the MEbrown module and gene set, supporting the reliability of the results (Table 1).

3.3 Prediction and Validation of TFs

Mining the binding sites for TFs using the UCSC database, followed by the screening of TFs using the JASPAR database, identified seven significant TFs. These TFs included JUNB, BACH2, TBP, ZNF384, RELA, PATZ1, ZNF460, and ZNF24. Of these, JUNB (R = 0.51, $p < 0.001$), TBP (R = 0.54, $p < 0.001$), ZNF384 (R = 0.62, $p < 0.001$), and ZNF460 (R = 0.5, $p < 0.001$) were strongly correlated with gene expression in the myocardial tissue (Fig. 6).

3.4 PPI and TF-Gene Regulatory Network

The constructed PPI network contained 21 nodes and 61 connection lines. We identified the central genes according to the "degree" method and found that *Cxcl1* had the highest linkage value, followed by *Ccl3*, *Ccl4*, *Ccl7*, *Cd14*, *Socs3*, and *Timp1*. These results are concordant with the results obtained by the intersection of the modules and immune infiltration data. Moreover, the set of hub genes identified by the cytohubba and MCODE plugins also contained these seven genes (Fig. 7).

Additionally, we determined the network of action between TFs, miRNAs, and hub genes. The node color and size were based on the strength of the relationship in the TF database. The TF-miRNA co-regulatory network comprised 133 nodes and 167 edges, where the nodes comprised seven hub genes, 72 miRNAs, and 54 TFs (Fig. 7).

3.5 Screening of Compound Molecules and Molecular Docking Simulation

The triggering and antagonistic drug molecules were identified based on the similarity between the expression profiles of DEG and small molecules. The closer the score value is to 100, the more similar the DEG is to the small-molecule treatment record, and the closer it is to –100, the more dissimilar the DEG is to the small-molecule treatment record. Chaetocin, auranofin, menadione, calyculin, rilmenidine, guanabenz, escitalopram, and nifedipine were the highest-scoring compounds (**Supplementary Table 1**). Nifedipine, the most likely CIR antagonist, successfully molecularly docked with proteins encoded by *Ccl3*, *Ccl4*, *Ccl7*, *Cd14*, *Cxcl1*, *Hspa1a*, and *Socs3*, with molecular binding energies of –5.4, –7.7, –4.2, –5.0, –6.0, –4.7, and –5.3 kcal/mol, respectively (Fig. 8).

3.6 Validation of DEG Expression 24 h after CIR in Vivo

The representative 2,3,5-triphenyl tetrazolium chloride staining images, infarct volume percentage, and neurological deficit score 24 h after MCAO/R are shown in Fig. 9. The mean percentage of cerebral infarct volume was 33.12%, and the average neurological deficit score was 2.33 in the MCAO/R group. The real-time PCR revealed remarkably higher expression of all DEGs (including *Ccl3*, *Ccl4*, *Ccl7*, *Cxcl1*, *Cd14*, *Socs3*, and *Hspa1a*) in the cortex tissues of the MCAO/R group than that in the cortex tissues of the sham group. Each DEG showed a significant statistical difference with $p < 0.0001$. *In vivo* validation results were consistent with those of our previous bioinformatic analysis (Fig. 9 and **Supplementary Fig. 2**). At the translational level, Western blot (WB) was used to detect the changed proteins of target protein expression. Compared with the normal group, the expression levels of *Ccl3*, *Ccl4*, *Ccl7*, *Hspa1a*, and *Socs3* were significantly changed in the CIR group; however, there were no significant differences in the expressions of *Cxcl1* and *Cd14* (Fig. 10). In addition, the immunohistochemistry results of CD14, SOCS3, and HSPA1A in human brain tissues and their localization in brain cells in the database clearly distinguished their expression levels and distribution in the nucleoplasm (**Supplementary Fig. 3**).

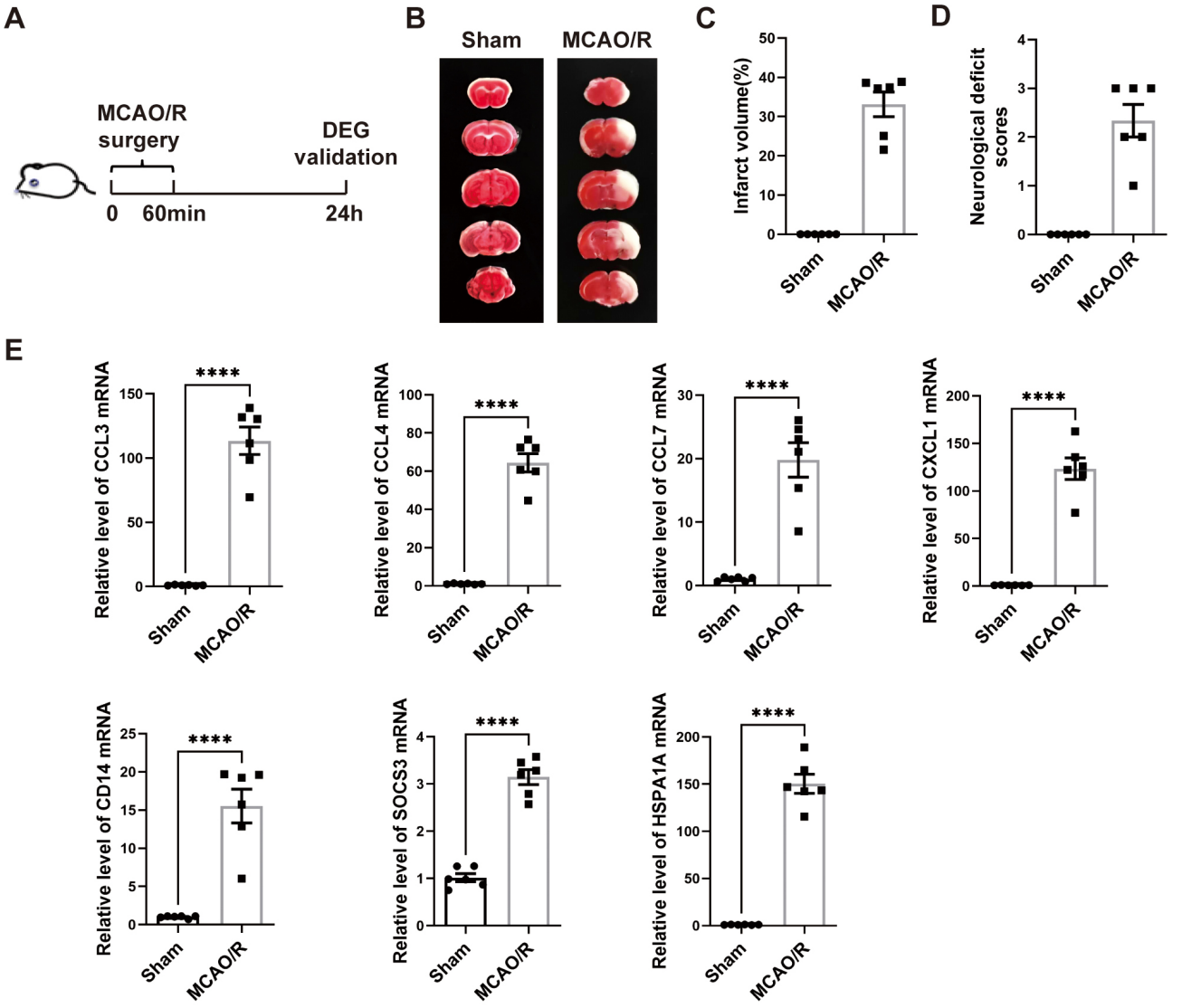

Fig. 9. Evaluation of animal models and real-time PCR results of hub gene expression validation. Tissues from successfully constructed ischemia-reperfused mice were subjected to RNA extraction, reverse transcription, and PCR to verify the differences in expression of individual genes. (A) The schematic representation of the model used in this study. (B) 2,3,5-Triphenyltetrazolium chloride staining images of brain sections. (C) proportion of infarct volume (n = 6), and (D) neurological deficit scores 24 h after middle cerebral artery occlusion and reperfusion (n = 6). (E) Expression of hub genes estimated using real-time PCR (n = 6, The data are shown as the means $\pm$ SEM, ****$p < 0.0001$, unpaired *t*-test).

4. Discussion

In this study, 25 DEGs and 6 gene modules were collected and constructed from 48 CIR samples and 16 sham surgery samples using the WGCNA method. After intersecting the immune gene dataset, 25 DEGs, and the most relevant gene set, 7 genes, namely *Ccl3*, *Ccl4*, *Ccl7*, *Cxcl1*, *Hspa1a*, *Cd14*, and *Socs3*, were considered pivotal. GSEA showed that the gene sets were significantly related to the acute inflammatory response, eosinophil chemotaxis, eosinophil migration, regulation of lymphocyte chemotaxis, and positive regulation of interleukin 1 β production. A PPI network was constructed using 21 nodes and 61 connection lines. We screened eight potential drug small molecules, including chaetocin, auranofin, menadione, calyculin, rilmenidine, guanabenz, escitalopram, and nifedipine, for the treatment of CIR and performed their molecular docking simulations. Finally, we validated the above results in a murine CIR model and performed real-time PCR to verify the expression of the selected genes.

We identified seven immune infiltration-associated genes for CIR: *Ccl3*, *Ccl4*, *Ccl7*, *Cxcl1*, *Hspa1a*, *Cd14*, and *Socs3*. *Cxcl1*, a member of the CXC chemokine family, is involved in inflammation, cell growth, and tumorigenesis [31–33]. CXCL1 is secreted by neutrophils, macrophages, and epithelial cells and serves as a neutrophil chemoattrac-

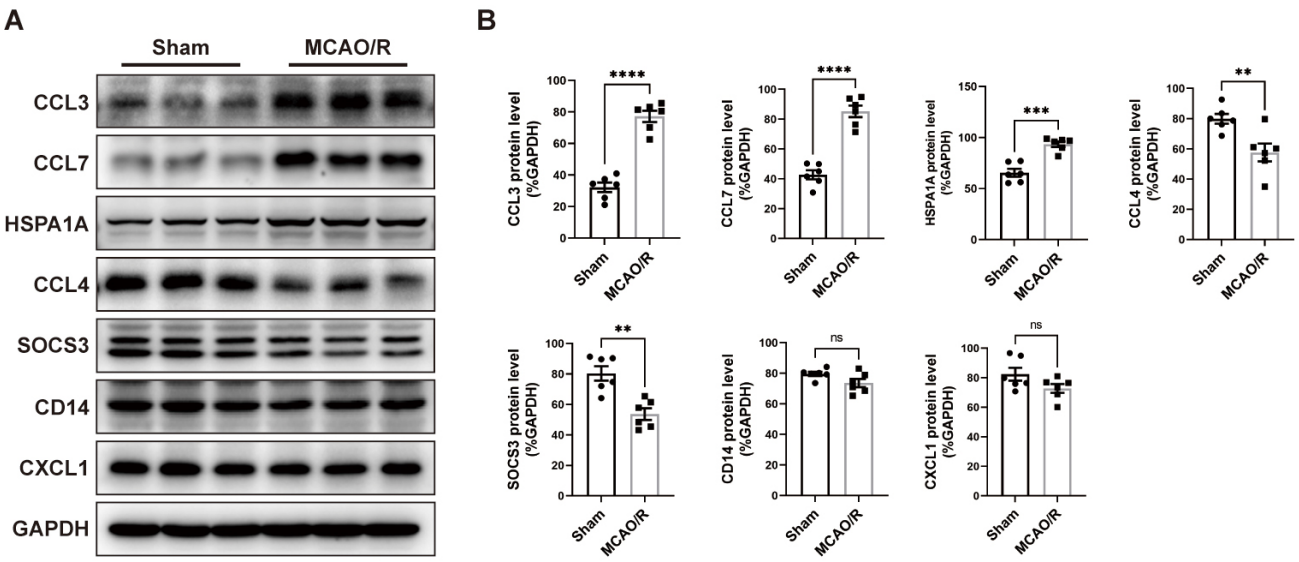

Fig. 10. Western blotting results of hub gene expression validation. Genes that reflect differential expression in PCR validation are validated at the translational level and presented quantitatively. (A) The expression levels of CCL3, CCL7, HSPA1A, CCL4, SOCS3, CD14 and CXCL1 were assessed by western blotting. (B) The protein levels were quantified by normalizing to the GAPDH levels (n = 6, The data are shown as the means ± SEM, $^{**}p < 0.01$, $^{***}p < 0.001$, $^{****}p < 0.0001$, ns, no significance, unpaired *t*-test).

tant [34]. Kaltenmeier *et al.* [35] speculated that CXCL1 plays a critical role in signaling neutrophil trafficking and migration during hepatic ischemia-reperfusion injury. In contrast, Gelderblom *et al.* [36] reported that CXCL1 levels in brain tissue were significantly elevated in mice with acute ischemic stroke. This finding is consistent with that of the present study. Furthermore, CXCL1 overexpression leads to neutrophil infiltration, resulting in disruption of the blood-brain barrier integrity through elastase secretion [37]. The potential of CXCL1 as a novel therapeutic target for CIR is evident. Shi *et al.* [38] reported that miRNA-532-5p upregulation reduced CIR injury by inhibiting the CXCL1/CXCR2/NF-κB signaling pathway. Blockade of the T cell Ig domain and mucin domain-1 was reported to ameliorate CIR by reducing the number of neutrophils, macrophage functionality, and CXCL1 levels [39]. Although these studies suggest the therapeutic potential of CXCL1, additional studies are required to confirm the speculations and validate CXCL1 as a promising therapeutic target in CIR.

The CCL is a member of the CC chemokine family [40]. CCLn (n denotes different numbers) is closely involved in inflammation and immune responses [41]. CCL7, also known as monocyte chemoattractant protein-3, serves as a chemoattractant for leukocytes, including monocytes, eosinophils, basophils, DC, natural killer cells, and T lymphocytes [42,43]. Owing to the low number of reports, the role of CCL7 in CIR remains unclear. To date, only one study has investigated CCL7 expression and function in CIR [40]. The study reported a notable increase in *Ccl7* mRNA levels in mice with CIR, paralleling leukocyte infiltration and accumulation following a stroke [44]. These findings are consistent with the results of the present study. CCL3 is an active inflammatory mediator in ischemic brain injury and serves as a chemoattractant for monocytes and neutrophils at inflammatory sites [45]. CCL3 upregulation is associated with monocytes and microglial infiltration in the ischemic brain [46]. CCL4 serves as a chemoattractant for monocytes at inflammatory sites [47]. Unfortunately, there have been no studies on the mechanisms of CCL3 and CCL4 in the CIR. We speculate that CCL3 and CCL4 might play roles similar to those of CCL7 in CIR; however, further investigation of CCL3, CCL4, and CCL7 in CIR is required.

SOCS3 is a regulator of the Janus kinase-signal transducer and activator of the transcription 3 signaling pathway [48]. Janus kinases-signal transducer and activator of transcription 3 signaling is activated after cerebral ischemia and induces an inflammatory response [49]. However, it remains controversial whether Janus kinases-signal transducer and activator of transcription 3 activation has a neuroprotective effect similar to *Socs3*. Liang *et al.* [50] reported that the expression of SOCS3 increased in CIR, and overexpression of SOCS3 inhibited STAT3 phosphorylation and inflammatory factor expression, exhibiting a neuroprotective effect. This finding of Liang *et al.* [50] is consistent with that of our study. Furthermore, Gly^{14}-humanin, a derivative of humanin, imparts a neuroprotective effect by alleviating apoptosis via reduced SOCS3 expression and increased STAT3 expression [51]. However, to understand the precise underlying mechanisms, further investigations are required.

The monocyte differentiation antigen, CD14, is a pattern recognition receptor that binds directly to lipopolysaccharide [52]. Previously, we considered CD14 to be a

monocyte marker. However, CD14 is a multifunctional receptor and is involved in various biological processes, including inflammation [53], cancer [54], and atherosclerosis [55]. CD14 is activated by inducible nitric oxide synthase in microglia and has been speculated to facilitate inflammatory responses after ischemic stroke via activation of the NF-κB pathway [53]. Moreover, CD14 deficiency has worsened stroke outcomes [56]. Therefore, we speculated that CD14 might be an important modulator of CIR. Further investigations of the molecular mechanisms underlying CD14 in CIR are required.

This study had several limitations. First, all data were obtained from the same dataset, and the sample size of the cited datasets was relatively small. Second, the experimental validation of upstream transcription factors has not been updated and is ongoing. Finally, the potential therapeutic chemicals for CIR were screened using a database. Therefore, the findings of the present study should be validated using further experiments.

5. Conclusions

In this study, we performed WGCNA on data from the GEO database to identify hub genes involved in CIR. We found that several hub genes, *Cxcl1*, *Ccl3*, *Ccl4*, *Ccl7*, *Socs3*, Cd14, and *Hspa1a*, are differentially expressed in CIR and normal tissue. Simultaneously, an experiment including transcription and translation level assays was carried out to confirm the status of these hub genes. The expression levels of *Ccl3*, *Ccl7*, and *Hspa1a* in CIR tissues were considerably greater than those in normal tissues, while *Ccl4*, and *Socs3* were the opposite of the former. Further, bioinformatic approaches were used to build regulatory networks of biomarkers and to search for possible therapeutic agents. This may provide insight into the treatment of ischemia-reperfusion injury in humans.

Abbreviations

CCL, C-C motif chemokine ligand; CIR, cerebral ischemia-reperfusion; DEG, differentially expressed gene; GEO, Gene Expression Omnibus; GO, Gene Ontology; GSEA, Gene Set Enrichment Analysis; KEGG, Kyoto Encyclopedia of Genes and Genomes; MCAO/R, middle cerebral artery occlusion and reperfusion; PPI, protein–protein interaction; SOCS, suppressor of cytokine signaling; TF, transcription factor; WGCNA, Weighted gene correlation network analysis.

Availability of Data and Materials

The datasets for this study can be found in the GEO.

Author Contributions

All authors contributed to the study conception and design. Material preparation and data collection were performed by AD and JW. The first draft of the manuscript was written by QG, and all authors commented on previous versions of the manuscript. XL, HP, GT, QG, AD, JW, LW, XZ, XY, SL, MS, QQ and IC established animal models and the tested model data. All authors contributed to editorial changes in the manuscript. All authors read and approved the final manuscript.

Ethics Approval and Consent to Participate

All animal experiments were performed in accordance with protocols approved by the Ethics Committee of Nanjing Medical University (Number : 1903016-1) and complied with the Guidelines of Laboratory Animals for Biomedical Research published by the National Institutes of Health.

Acknowledgment

The authors thank the patients and investigators who participated in GEO for providing the data and Jiajin Chen, Department of Biostatistics, School of Public Health, Nanjing Medical University, for providing statistical guidance.

Funding

This research was supported by the Key R&D Project through the Science and Technology Department of Zhejiang Province (grant number: 2020C03018).

Conflict of Interest

The authors declare no conflict of interest.

Supplementary Material

Supplementary material associated with this article can be found, in the online version, at https://doi.org/10.31083/j.fbl2808179.

References

[1] Edsfeldt A, Swart M, Singh P, Dib L, Sun J, Cole JE, *et al*. Interferon regulatory factor-5-dependent CD11c+ macrophages contribute to the formation of rupture-prone atherosclerotic plaques. European Heart Journal. 2022; 43: 1864–1877.

[2] Tsao CW, Aday AW, Almarzooq ZI, Alonso A, Beaton AZ, Bittencourt MS, *et al*. Heart Disease and Stroke Statistics-2022 Update: A Report From the American Heart Association. Circulation. 2022; 145: e153–e639.

[3] Kuriakose D, Xiao Z. Pathophysiology and Treatment of Stroke: Present Status and Future Perspectives. International Journal of Molecular Sciences. 2020; 21: 7609.

[4] National Institute of Neurological Disorders and Stroke rt-PA Stroke Study Group. Tissue plasminogen activator for acute ischemic stroke. The New England Journal of Medicine. 1995; 333: 1581–1587.

[5] Goyal M, Menon BK, van Zwam WH, Dippel DWJ, Mitchell PJ, Demchuk AM, *et al*. Endovascular thrombectomy after large-vessel ischaemic stroke: a meta-analysis of individual patient data from five randomised trials. Lancet (London, England). 2016; 387: 1723–1731.

[6] Saver JL, Goyal M, van der Lugt A, Menon BK, Majoie CBLM, Dippel DW, *et al*. Time to Treatment With Endovascular

Thrombectomy and Outcomes From Ischemic Stroke: A Meta-analysis. Journal of the American Medical Association. 2016; 316: 1279–1288.
[7] Chomova M, Zitnanova I. Look into brain energy crisis and membrane pathophysiology in ischemia and reperfusion. Stress. 2016; 19: 341–348.
[8] He G, Xu W, Tong L, Li S, Su S, Tan X, *et al*. Gadd45b prevents autophagy and apoptosis against rat cerebral neuron oxygen-glucose deprivation/reperfusion injury. Apoptosis: an International Journal on Programmed Cell Death. 2016; 21: 390–403.
[9] Zhang W, Song JK, Zhang X, Zhou QM, He GR, Xu XN, *et al*. Salvianolic acid A attenuates ischemia reperfusion induced rat brain damage by protecting the blood brain barrier through MMP-9 inhibition and anti-inflammation. Chinese Journal of Natural Medicines. 2018; 16: 184–193.
[10] Chamorro Á, Meisel A, Planas AM, Urra X, van de Beek D, Veltkamp R. The immunology of acute stroke. Nature Reviews. Neurology. 2012; 8: 401–410.
[11] Franke M, Bieber M, Kraft P, Weber ANR, Stoll G, Schuhmann MK. The NLRP3 inflammasome drives inflammation in ischemia/reperfusion injury after transient middle cerebral artery occlusion in mice. Brain, Behavior, and Immunity. 2021; 92: 223–233.
[12] Mracsko E, Veltkamp R. Neuroinflammation after intracerebral hemorrhage. Frontiers in Cellular Neuroscience. 2014; 8: 388.
[13] Mracsko E, Javidi E, Na SY, Kahn A, Liesz A, Veltkamp R. Leukocyte invasion of the brain after experimental intracerebral hemorrhage in mice. Stroke. 2014; 45: 2107–2114.
[14] Lakhan SE, Kirchgessner A, Hofer M. Inflammatory mechanisms in ischemic stroke: therapeutic approaches. Journal of Translational Medicine. 2009; 7: 97.
[15] Gill D, Veltkamp R. Dynamics of T cell responses after stroke. Current Opinion in Pharmacology. 2016; 26: 26–32.
[16] Na SY, Mracsko E, Liesz A, Hünig T, Veltkamp R. Amplification of regulatory T cells using a CD28 superagonist reduces brain damage after ischemic stroke in mice. Stroke. 2015; 46: 212–220.
[17] Cheng X, Yang YL, Li WH, Liu M, Wang YH, Du GH. Cerebral ischemia-reperfusion aggravated cerebral infarction injury and possible differential genes identified by RNA-Seq in rats. Brain Research Bulletin. 2020; 156: 33–42.
[18] Zhang ZH, Wang YR, Li F, Liu XL, Zhang H, Zhu ZZ, *et al*. Circ-camk4 involved in cerebral ischemia/reperfusion induced neuronal injury. Scientific Reports. 2020; 10: 7012.
[19] Nieuwenhuis TO, Yang SY, Verma RX, Pillalamarri V, Arking DE, Rosenberg AZ, *et al*. Consistent RNA sequencing contamination in GTEx and other data sets. Nature Communications. 2020; 11: 1933.
[20] Langfelder P, Horvath S. WGCNA: an R package for weighted correlation network analysis. BMC Bioinformatics. 2008; 9: 559.
[21] Wan Q, Tang J, Han Y, Wang D. Co-expression modules construction by WGCNA and identify potential prognostic markers of uveal melanoma. Experimental Eye Research. 2018; 166: 13–20.
[22] Shi Z, Derow CK, Zhang B. Co-expression module analysis reveals biological processes, genomic gain, and regulatory mechanisms associated with breast cancer progression. BMC Systems Biology. 2010; 4: 74.
[23] Islam R, Ahmed L, Paul BK, Ahmed K, Bhuiyan T, Moni MA. Identification of molecular biomarkers and pathways of NSCLC: insights from a systems biomedicine perspective. Journal, Genetic Engineering & Biotechnology. 2021; 19: 43.
[24] Wang M, Wang L, Pu L, Li K, Feng T, Zheng P, *et al*. LncRNAs related key pathways and genes in ischemic stroke by weighted gene co-expression network analysis (WGCNA). Genomics. 2020; 112: 2302–2308.
[25] Hasan MT, Hassan M, Ahmed K, Islam MR, Islam K, Bhuyian T, *et al*. Network based study to explore genetic linkage between diabetes mellitus and myocardial ischemia: bioinformatics approach. Gene Reports. 2020; 21: 100809.
[26] Puspo NA, Akter L, Siddique S, Paul BK, Ahmed K, Bhuiyan, T, *et al*. Analyzing the protein-protein interaction network and the topological properties of prostate cancer and allied diseases: a computational bioinformatics approach. Gene Reports. 2020; 21: 100842.
[27] Islam MN, Shaolin SS, Paul BK, Islam M, Ahmed KJGR. Mining and predicting protein-drug interaction network of breast cancer risk genes. Gene Reports. 2020; 20: 100753.
[28] Khan T, Paul BK, Hasan MT, Islam MR, Arefin MA, Ahmed K, *et al*. Significant pathway and biomarker identification of pancreatic cancer associated lung cancer. Informatics in Medicine Unlocked. 2021; 25: 100637.
[29] Arac A, Brownell SE, Rothbard JB, Chen C, Ko RM, Pereira MP, *et al*. Systemic augmentation of alphaB-crystallin provides therapeutic benefit twelve hours post-stroke onset via immune modulation. Proceedings of the National Academy of Sciences of the United States of America. 2011; 108: 13287–13292.
[30] Longa EZ, Weinstein PR, Carlson S, Cummins R. Reversible middle cerebral artery occlusion without craniectomy in rats. Stroke. 1989; 20: 84–91.
[31] Luster AD. Chemokines–chemotactic cytokines that mediate inflammation. The New England Journal of Medicine. 1998; 338: 436–445.
[32] Lira SA, Furtado GC. The biology of chemokines and their receptors. Immunologic Research. 2012; 54: 111–120.
[33] Wang JM, Deng X, Gong W, Su S. Chemokines and their role in tumor growth and metastasis. Journal of Immunological Methods. 1998; 220: 1–17.
[34] Omari KM, Lutz SE, Santambrogio L, Lira SA, Raine CS. Neuroprotection and remyelination after autoimmune demyelination in mice that inducibly overexpress CXCL1. The American Journal of Pathology. 2009; 174: 164–176.
[35] Kaltenmeier C, Wang R, Popp B, Geller D, Tohme S, Yazdani HO. Role of Immuno-Inflammatory Signals in Liver Ischemia-Reperfusion Injury. Cells. 2022; 11: 2222.
[36] Gelderblom M, Weymar A, Bernreuther C, Velden J, Arunachalam P, Steinbach K, *et al*. Neutralization of the IL-17 axis diminishes neutrophil invasion and protects from ischemic stroke. Blood. 2012; 120: 3793–3802.
[37] Ikegame Y, Yamashita K, Hayashi SI, Yoshimura SI, Nakashima S, Iwama T. Neutrophil elastase inhibitor prevents ischemic brain damage via reduction of vasogenic edema. Hypertension Research: Official Journal of the Japanese Society of Hypertension. 2010; 33: 703–707.
[38] Shi Y, Yi Z, Zhao P, Xu Y, Pan P. MicroRNA-532-5p protects against cerebral ischemia-reperfusion injury by directly targeting CXCL1. Aging. 2021; 13: 11528–11541.
[39] Zheng Y, Wang L, Chen M, Liu L, Pei A, Zhang R, *et al*. Inhibition of T cell immunoglobulin and mucin-1 (TIM-1) protects against cerebral ischemia-reperfusion injury. Cell Communication and Signaling: CCS. 2019; 17: 103.
[40] Geng H, Chen L, Tang J, Chen Y, Wang L. The Role of CCL2/CCR2 Axis in Cerebral Ischemia-Reperfusion Injury and Treatment: From Animal Experiments to Clinical Trials. International Journal of Molecular Sciences. 2022; 23: 3485.
[41] Christopherson K, 2nd, Hromas R. Chemokine regulation of normal and pathologic immune responses. Stem Cells (Dayton, Ohio). 2001; 19: 388–396.
[42] Loetscher P, Seitz M, Clark-Lewis I, Baggiolini M, Moser B. Monocyte chemotactic proteins MCP-1, MCP-2, and MCP-3 are major attractants for human CD4+ and CD8+ T lymphocytes.

FASEB Journal: Official Publication of the Federation of American Societies for Experimental Biology. 1994; 8: 1055–1060.
[43] Van Coillie E, Van Damme J, Opdenakker G. The MCP/eotaxin subfamily of CC chemokines. Cytokine & Growth Factor Reviews. 1999; 10: 61–86.
[44] Wang X, Li X, Yaish-Ohad S, Sarau HM, Barone FC, Feuerstein GZ. Molecular cloning and expression of the rat monocyte chemotactic protein-3 gene: a possible role in stroke. Brain Research. Molecular Brain Research. 1999; 71: 304–312.
[45] Montecucco F, Steffens S, Burger F, Da Costa A, Bianchi G, Bertolotto M, *et al*. Tumor necrosis factor-alpha (TNF-alpha) induces integrin CD11b/CD18 (Mac-1) up-regulation and migration to the CC chemokine CCL3 (MIP-1alpha) on human neutrophils through defined signalling pathways. Cellular Signalling. 2008; 20: 557–568.
[46] Cowell RM, Xu H, Galasso JM, Silverstein FS. Hypoxic-ischemic injury induces macrophage inflammatory protein-1alpha expression in immature rat brain. Stroke. 2002; 33: 795–801.
[47] Montecucco F, Burger F, Mach F, Steffens S. CB2 cannabinoid receptor agonist JWH-015 modulates human monocyte migration through defined intracellular signaling pathways. American Journal of Physiology. Heart and Circulatory Physiology. 2008; 294: H1145–H1155.
[48] Gao Y, Zhao H, Wang P, Wang J, Zou L. The roles of SOCS3 and STAT3 in bacterial infection and inflammatory diseases. Scandinavian Journal of Immunology. 2018; 88: e12727.
[49] Satriotomo I, Bowen KK, Vemuganti R. JAK2 and STAT3 activation contributes to neuronal damage following transient focal cerebral ischemia. Journal of Neurochemistry. 2006; 98: 1353–1368.
[50] Liang E, Li X, Fu W, Zhao C, Yang B, Yang Z. COP9 Signalosome Subunit 3 Restricts Neuroinflammatory Responses During Cerebral Ischemia/Reperfusion Injury Through Stabilizing Suppressor of Cytokine Signaling 3 Protein. Neuropsychiatric Disease and Treatment. 2021; 17: 1217–1227.
[51] Gao G, Fan H, Zhang X, Zhang F, Wu H, Qi F, *et al*. Neuroprotective effect of G^{14}-humanin on global cerebral ischemia/reperfusion by activation of SOCS3 - STAT3 - MCL-1 signal transduction pathway in rats. Neurological Research. 2017; 39: 895–903.
[52] Wu Z, Zhang Z, Lei Z, Lei P. CD14: Biology and role in the pathogenesis of disease. Cytokine & Growth Factor Reviews. 2019; 48: 24–31.
[53] Zhou M, Wang CM, Yang WL, Wang P. Microglial CD14 activated by iNOS contributes to neuroinflammation in cerebral ischemia. Brain Research. 2013; 1506: 105–114.
[54] Kuo WT, Lee TC, Yang HY, Chen CY, Au YC, Lu YZ, *et al*. LPS receptor subunits have antagonistic roles in epithelial apoptosis and colonic carcinogenesis. Cell Death and Differentiation. 2015; 22: 1590–1604.
[55] An D, Hao F, Zhang F, Kong W, Chun J, Xu X, *et al*. CD14 is a key mediator of both lysophosphatidic acid and lipopolysaccharide induction of foam cell formation. The Journal of Biological Chemistry. 2017; 292: 14391–14400.
[56] Janova H, Böttcher C, Holtman IR, Regen T, van Rossum D, Götz A, *et al*. CD14 is a key organizer of microglial responses to CNS infection and injury. Glia. 2016; 64: 635–649.